Contents lists available at ScienceDirect

Materials Today Bio

journal homepage: www.journals.elsevier.com/materials-today-bio

Acceleration of burn wound healing by micronized amniotic membrane seeded with umbilical cord-derived mesenchymal stem cells

Zixuan Zhou [a,1], Jingnan Xun [a,1], Chenghao Wu [b,1], Chao Ji [a,1], Shizhao Ji [a,1], Futing Shu [a], Yuxiang Wang [a], Hao Chen [a], Yongjun Zheng [a,*], Shichu Xiao [a,**]

[a] Department of Burn Surgery, The First Affiliated Hospital of Naval Medical University, Shanghai, 200433, People's Republic of China
[b] Department of Obstetrics and Gynecology, Tongji Hospital, Tongji University School of Medicine, Shanghai, 200065, People's Republic of China

ARTICLE INFO

ABSTRACT

Umbilical cord-derived mesenchymal stem cells (UC-MSC) are promising candidates for wound healing. However, the low amplification efficiency of MSC in vitro and their low survival rates after transplantation have limited their medical application. In this study, we fabricated a micronized amniotic membrane (mAM) as a microcarrier to amplify MSC in vitro and used mAM and MSC (mAM-MSC) complexes to repair burn wounds. Results showed that MSC could live and proliferate on mAM in a 3D culture system, exhibiting higher cell activity than in 2D culture. Transcriptome sequencing of MSC showed that the expression of growth factor-related, angiogenesis-related, and wound healing-related genes was significantly upregulated in mAM-MSC compared to traditional 2D-cultured MSC, which was verified via RT-qPCR. Gene ontology (GO) analysis of differentially expressed genes (DEGs) showed significant enrichment of terms related to cell proliferation, angiogenesis, cytokine activity, and wound healing in mAM-MSC. In a burn wound model of C57BL/6J mice, topical application of mAM-MSC significantly accelerated wound healing compared to MSC injection alone and was accompanied by longer survival of MSC and greater neovascularization in the wound.

1. Introduction

In accordance with a report by the World Health Organization in 2018, an estimated 180 000 deaths every year are caused by burns, and the vast majority occur in low-and-middle-income countries (https://www.who.int/news-room/fact-sheets/detail/burns). Burn wounds consist of three distinguished zones of coagulation, stasis, and hyperemia (Jackson's burn wound model), and have four specific characteristics: more inanimate tissues, more exudates, more susceptible to infection, and easier to leave scars [1,2]. The pathophysiological process of burn wound healing is intricate and dynamic, including three interrelated and overlapping phases of hemostasis/inflammation, proliferation and remodeling [3–5]. In clinical practice, early surgical debridement of the inanimate tissues followed by grafting are still the gold-standard for deep extensive burn wound care [6]. However, for patients with large-scale burns, the contradiction between the "supply" and "demand" of autologous skin transplantation remains the main obstacle. With the

development and innovations in stem cell therapy and skin substitutes, stem cell-based biomaterials have been widely studied to promote burn wound repair and skin tissue regeneration, showing good application prospects.

Mesenchymal stem cells (MSC) derived from adipose, bone marrow, human umbilical cord or other tissues, and their exosomes or extracellular vesicles have been recommended as potential candidates for the wound repair because of their therapeutic properties, including anti-inflammatory and immunomodulatory potentials [7,8], regenerative capability [9], re-epithelialization [10] and neovascularization [11]. MSC transplantation can accelerate wound healing in all stages and prevent wound contracture and scar formation [12]. According to the current literature, MSCs have been widely employed in preclinical animal studies and clinical trials, and most of them suggest that MSCs are safe and promising therapeutic means [13–16]. A recent randomized clinical study demonstrated that adipose derived MSC therapy enhanced healing rate of skin wounds by increasing the granulation tissue coverage

* Corresponding author.
** Corresponding author.
  E-mail addresses: smmuzhengyongjun@163.com (Y. Zheng), huangzhuoxiao@sohu.com (S. Xiao).
[1] These authors contributed equally to this article.

rate and thickness of granulation tissue [17]. Another open-label single-arm clinical trial published in 2022 showed that skin-derived ABCB5^{+} MSCs accelerated wound healing of diabetic foot ulcers by increasing capillary proliferation and vascularization [18]. These studies imply that MSC therapy will be a hopeful and essential approach for skin wound healing in the future. However, several obstacles limit their practical applications. First, cells are traditionally cultured in two-dimensional plates, and this culture method often leads to slow proliferation, low activity, easy differentiation, and even loss of the therapeutic potency of MSC because the plates cannot mimic the microenvironment in which stem cells live and proliferate *in vivo* [19–21]. Second, during the delivery of MSC, cells are generally injected intravenously for systemic distribution or are injected locally into target tissues, and shear stress during injection may damage the cells [22]. Third, because of the more inanimate tissues and exudates in the burn wound microenvironment, it is not beneficial for the survival and proliferation of stem cells in the harsh wound environment [23]. Consequently, stem cells have difficulty in performing their therapeutic functions. To overcome these obstacles, additional strategies must be employed to achieve optimal application of MSC.

Microcarriers with 3D culture systems provide new ideas to address the aforementioned problems occurring in traditional cell culture, delivery, and therapeutic processes. This method has undergone several innovations to satisfy different demands [24]. Microcarriers can provide larger and more surface matrices for MSC to adhere to and proliferate compared to 2D plates [25]. Tan et al. verified that MSC seeded in CultiSpher S microcarriers proliferate quickly and with high cell viability [26]. Moreover, this 3D cell culture strategy can contribute to the longer survival and more effective therapeutic applications of MSC [19,22,27]. Kim et al. showed that the secretion and bioactivity of UC-MSC-derived extracellular vesicles could be enhanced by 3D culture [28]. Zeng et al. discovered that preformed gelatin microcryogels, as injectable cell carriers, enhanced the survival of MSC *in vivo* and accelerated skin wound healing [29]. Researchers have used synthetic polymers, such as polystyrene, plastic, or glass, as microcarriers to increase the expansion efficiency of stem cells; however, these microcarriers pose challenges in the downstream process [30]. For example, these synthetic materials cannot degrade *in vivo*; therefore, stem cells need to be digested to separate them from the microcarriers before use, resulting in the loss of cell viability. To solve this problem, it is necessary to investigate new microcarriers that can not only have excellent biocompatibility to support the proliferation of MSC but can also be transported directly into wounds.

The human amniotic membrane can meet these requirements and is expected to be a good microcarrier for MSC. The amniotic membrane contains type I-VII collagen, laminin, integrins, and other ECM components that can mimic the *in vivo* microenvironment, providing a "fertile soil" for stem cells to live and proliferate. In addition, the human amniotic membrane, a natural tissue from the placenta with excellent biocompatibility, can be applied directly *in vivo,* so that MSC need not be digested before use. Furthermore, the amniotic membrane plays a coordinated role with MSC to promote burn wound healing. The properties of the human amniotic membrane in promoting wound healing, skin tissue reconstruction, and regulating inflammation and microbial growth have been widely recognized by hundreds of clinical trials or pre-clinical papers, including the domains of burns and chronic ulcer treatment, peritoneal reconstruction, tendon repair, microvascular reconstruction, and corneal repair [31–40]. In our previous studies, we made great progress in upgrading the preparation methods for human amniotic membranes and found that decellularized amniotic membranes could be used to construct natural microcarriers for stem cells. Zheng et al. found that cryopreserved living micronized amniotic tissue can modulate the local microenvironment of diabetic wounds, thereby accelerating healing in mice [41]. Ji et al. prepared a cell niche for epidermal stem cells using an engineered human amniotic membrane, which acted as a dermal scaffold for healing and regeneration of full-thickness skin defects in mice [42].

In this study, we proposed the use of a natural human amniotic membrane to fabricate microcarriers called micronized amniotic membrane (mAM) to amplify UC-MSC in a 3D culture system. The mAM microcarrier was used to investigate the amplification efficiency and maintenance of MSC function *in vitro*. Finally, after applying mAM-MSC to burn wounds, their functions and mechanisms in accelerating wound repair were explored. mAM not only has the general characteristics of microcarriers, such as a large specific surface area, but also provides the natural cell niche to simulate the *in vivo* cell growth microenvironment, thus promoting the adhesion, growth, and the biological functions of MSC. In addition, the mechanical properties of mAM allow MSC to be conveniently delivered and glued onto wounds by just smearing mAM-MSC on the wound surface without injection, reducing the harm caused by shear stress from injection. The natural cell niche provided by mAM could protect MSC from tolerating ischemic and hypoxic conditions in the burn wound after transplantation, thus promoting the survival of MSC.

2. Materials and methods

2.1. Study design and ethical considerations

The objectives of this study were to analyze the impact of mAM as a microcarrier to amplify MSC *in vitro* and used mAM and MSC complexes to repair burn wounds. All *in vitro* experiments were divided into 2D-cultured MSC (MSC) group and 3D-cultured MSC group (mAM-MSC) to compare the differences of cell proliferation, growth and paracrine function. For *in vivo* experiments, 6–8 weeks C57BL/6 mice were used with 12 mice per group to ensure statistical power and deep second-degree burn wounds were created on each side of the dorsal skin. Number of repeats was specified in each figure legend. This study was approved by the Ethics Committee of Changhai Hospital, Shanghai, China, and conducted according to the animal use and care committee of Changhai Hospital.

2.2. Fabrication of mAM

All procedures were approved by the Ethics Committee of Changhai Hospital (Shanghai, China), and informed consent was obtained from all donors. Placental tissue from healthy donors was obtained within 24 h of cesarean section. First, the amniotic and chorionic membranes were separated using blunt separation. Then the amniotic membrane was washed with phosphate-buffered saline (PBS) and stored in PBS containing 10% dimethyl sulfoxide (DMSO) at $-80\,^\circ$C. The cellular and DNA components of the amniotic membrane were eliminated by three repetitive freeze-thaw cycles and digestion with 1 mg/mL DNase (Sigma, USA) using our previously described methods [42]. Decellularized amniotic membrane was homogenized into microparticles about 400 μm in size by a peeler and freeze-dried to produce mAM.

2.3. Isolation and culture of UC-MSC

The obtained umbilical cords were washed with PBS and cut into 2 cm long pieces. The umbilical vein was peeled off from each piece, together with the two arteries. The remainder is mainly Wharton's jelly. Wharton's jelly was cut into blocks approximately 1 mm in size and placed in a culture dish. The dish was placed in an incubator for 2 h, and then complete medium was dropped slowly. The tissue was left undisturbed for 7 days in a 37 $^\circ$C incubator with 5% CO_2. Subsequently, cells could be seen migrated out of the tissue blocks. When cells reached 80–90% confluence, the primary cells were collected and passaged. Passage 3–5 cells were used in subsequent experiments.

2.4. Construction of mAM-MSC

A 3D culture system was used to construct mAM-MSC. 30 mL of MSC suspension (5×10^4 cells/mL) together with 300 mg mAM were added to

the 3D culture system, and the rotation mode was set at 35 rpm for 5 min, 0 rpm for 1 h, for 24 cycles on day 0 and changed to a constant speed mode of 40 rpm after day 0. Subsequently, the samples were harvested for scanning electron microscopy (SEM), cytoskeleton staining, Cell Counting Kit-8 (CCK8) assay, live/dead staining, RT-qPCR, and RNA sequencing (RNA-seq).

2.5. Scanning electron microscopy (SEM)

The mAM-MSC in 3D culture system on day 3 post seeding was collected, rinsed three times in PBS, fixed in 2.5% glutaraldehyde for 2 h, and then cleaned once more with PBS. The mAM-MSC and mAM specimens were sprayed with gold and observed by SEM after dehydration with ethanol and tertiary butyl alcohol. Images of the two groups were captured using a scanning electron microscope (TM4000PLUS II, Hitachi, Japan). At least three replicates were used for each experiment.

2.6. Cytoskeleton staining

Cytoskeleton staining was used to visualize the cell morphology and structure. The mAM-MSC cultured for 3 and 7 days were collected and stained with phalloidin (Phalloidin-iFluor 594, Abcam, USA). First, mAM-MSC were fixed with paraformaldehyde (4%, PFA) for 10 min and then permeabilized with Triton X-100 (0.5%) for 5 min. After cleaning mAM-MSC with PBS, they were incubated with phalloidin for 30 min at room temperature in the dark. Finally, a DAPI solution (Wako Pure Chemical Industries, Japan) was used to stain the cell nuclei. A confocal microscope (Olympus, Tokyo, Japan) was used to observe fluorescence.

2.7. Viability and proliferation detection of mAM-MSC

To verify the viability and proliferation of mAM-MSC in the 3D culture system, CCK-8 assay and live/dead staining were conducted. A LIVE/DEAD Viability/Cytotoxicity Kit (Invitrogen, USA) was used to detect the cytoviability of MSC on mAM using fluorescence microscopy (Leica, Germany). mAM-MSC samples were collected from the 3D culture system on days 1, 3, and 7 for the cell proliferation assay using a CCK-8 kit (Dojindo, Japan) according to the manufacturer's instructions. The control group consisted of MSC cultured in 12-well plates, with 1 mL MSC suspension (5×10^4 cells/mL) added to each well. For the mAM-MSC group, 30 mL of MSC suspension (5×10^4 cells/mL) and 300 mg of mAM were co-cultured in a 3D culture system. 1 mL of suspension was drawn from the 3D culture system and transferred into one well of a 12-well plate. One hundred microliters of CCK8 were added to each well of both groups for incubation of up to 2 h. Subsequently, 100 μL of supernatant was aspirated from each well and put in wells of a 96-well plate. Absorbance was measured at 450 nm using a microplate reader (Biotek, USA). Three replicates were analyzed for each treatment group at each time point.

2.8. Transcriptomic analysis

The mAM-MSC samples cultured for 3 days in the 3D culture system were collected and marked as the mAM-MSC group (n = 3), whereas MSC cultured in 12-well plates were used as the control and marked as the MSC group (n = 3). Total RNA was extracted from each sample using TRIzol reagent (Invitrogen, USA). RNA libraries were constructed, and transcriptomic sequencing was performed by OE Biotech Co., Ltd. (China). For data analysis, DEGs were identified using DESeq. P value < 0.05 and fold change >1.5 or <0.5 were considered significant. Gene ontology (GO) enrichment, Kyoto Encyclopedia of Genes and Genomes (KEGG) pathway enrichment analysis, and Gene Set Enrichment Analysis (GSEA) were performed for in-depth bioinformatics analysis.

2.9. Quantitative real-time PCR

TRIzol reagent (Invitrogen, USA) was used to extract RNA from 2D-cultured MSC, mAM-MSC, and mouse burn wound tissues according to the manufacturer's instructions. *M*-MLV reverse transcription reagents (Takara, Japan) were used to reverse transcribe the cDNA. Real-time PCR was performed on a CFX96 (Bio-Rad, USA) using an SYBR premix qPCR kit (Takara, Japan). The primer sequences are presented in Table 1.

2.10. Evaluation of the biological effects of mAM-MSC on HUVEC

The biological effects of mAM-MSC on HUVEC, including migration and angiogenesis, were evaluated using transwell and tube formation assays. The mAM-MSC was cultured in 3D culture system firstly with complete medium (DMEM containing 10% FBS) for 72 h and then switched to serum-free DMEM. After 48 h, the supernatant was collected, centrifuged, and filtered for subsequent experiments. Supernatants of the 2D-cultured MSC were collected in the same manner. DMEM was used as the negative control.

2.10.1. Cell migration assay

A 24-well transwell chamber (8 mm pore size, Corning, USA) was used to conduct the cell migration assay. The bottom chamber was filled with 600 μL supernatant of 2D-cultured MSC, supernatant of mAM-MSC, and DMEM (negative control group, NC group), in that order. HUVECs (1 $\times 10^5$ HUVECs diluted in serum-free high-glucose DMEM) were seeded in the upper chamber. After 24 h, cells in the upper layer of the membrane were wiped with swabs, and the migrated cells were stained with 0.1% crystal violet (Sigma, USA) after fixation with 4% PFA. Stained cells were observed under a light microscope (Leica, Germany), and cells from at least three wells were counted using ImageJ software (NIH, USA) for each group.

2.10.2. Tube formation assay

Fifty microliters of Matrigel (5 mg/mL, BD Biosciences, USA) were added to each well of a 96-well plate and allowed to solidify at 37 °C. Then, 4×10^4 HUVECs resuspended in 100 μL supernatant of 2D-cultured MSC, supernatant of mAM-MSC, and DMEM, in order, were seeded on the Matrigel of each well. After 4 h, cells were observed under a light microscope (Leica, Germany) and photographed. Vascularization was reflected by counting the number of nodes and the total length of the tubes.

Table 1
Primer sequences.

Gene	Forward (5′-3′)	Reverse (5′-3′)
Human VEGF	CAGGGAAGAGGAGGAGATG	CTGGGTTTGTCGGTGTTC
Human TGFB1	ACCTCGGCTGGAAGTGG	CCGGGTTATGCTGGTTGT
Human IGF1	CCCTGGACAATCAGACGAA	GTCGCAAACCGAACAGC
Human ANGPT1	CAATGGTCTCACGTTCTCAC	CCCGTAAGTCAGATGTTGTTT
Human GAPDH	GGTCACCAGGGCTGCTTTTA	GGATCTCGCTCCTGGAAGATG
Mice VEGF	AGCTTCCTACAGCACAGCAG	CACAGTGAACGCTCCAGGAT
Mice TGFB1	TTGGCCATGAATTTGACCTC	ACATCAGTCTCATTCACAGC
Mice ANGPT1	GGAGTCGGCATGAATCGCT	GAATGGGATCCCCCTCGG
Mice HGF	TACTCAGCGTCACAGCATGG	GCAGGACCGGCACAAGTC
Mice IGF1	GCTGCTGGCTTCTAAGTGTG	ACTGCCCAGTTCGTTTCAG
Mice MMP8	CAACCCCATCCAACCTACT	GAAGGGCCAGAACAGAGAT
Mice GAPDH	GGTCGGTGTGAACGGATTTG	TGTAGACCATGTAGTTGAGGTCA

VEGF: vascular endothelial growth factor; TGFB1: transforming growth factor-b1; IGF1: insulin-like growth factor-1; ANGPT1: angiopoietin-1; HGF: hepatocyte growth factor; MMP8: matrix metallopeptidase 8.

2.11. Preparation of Luc $^+$ MSC

Lentiviruses expressing luciferase (Luc) from Hanbio Tech (China) were used to infect MSC when the cells reached 30–50% confluency in a 6-well plate. At the same time, polybrene (Hanbio Tech, China) was added into each well to reach an ultimate concentration of 6 μg/mL, and then, the plate was shaken and incubated overnight at 37 °C. After incubation, the medium containing lentiviruses was removed, and complete medium was added. After amplification for one passage, positive cells (Luc$^+$) were collected and purified using puromycin (Sigma, USA). Luc$^+$ MSC from passage 4–6 were utilized for bioluminescence imaging experiments.

2.12. Burn wound model and treatment

Male C57BL/6 mice (aged 6–8 weeks) were obtained from SLAC Laboratory Animal Co., Ltd. (Shanghai, China), and animal experiments were approved by the Institutional Animal Care and Use Committee of the Naval Medical University, Shanghai, China. Mice were randomly and equally divided into four groups: mAM-MSC, mAM, MSC, and sham. After isoflurane inhalation anesthesia and hair removal, a deep second-degree burn wound was created on each side of the dorsal skin. In brief, a copper rod (1 cm in diameter, heated to 100 °C) was applied to burn the dorsal skin of the mice for 5 s [43]. After 48 h, a wound 1 cm in diameter was formed after the inanimate tissue was surgically removed from healthy skin, and this time point was marked as day 0. A donut-shaped silicone sheet was interrupted to the wound edge by 4–0 sutures to prevent contraction of the skin surrounding the wound, so that the wound healing rate could be monitored and measured objectively. The mAM-MSC and mAM were spread on the wound surface in the mAM-MSC and mAM groups, respectively. The number of cells in the mAM-MSC group was calculated using a NucleoConuter NC-200 (ChemoMetec, Denmark) [44,45], and the cell number in mAM-MSC was adjusted to 5×10^5. In the MSC group, cells resuspended in 100 μL PBS were subcutaneously injected around each wound at four sites. The number of cells applied to each wound site was 5×10^5. All wounds were covered with a transparent silicone film to prevent drying. The bandage integrity was assessed daily. Photographs of each wound in the four groups were taken at every time point, and the remaining wound area was calculated using ImageJ software (NIH, USA). The remaining wound area (%) = $S_r/S_i \times 100\%$, where S_i is the initial wound area on day 0, and S_r is the remaining wound area on days 3, 7, and 11. On day 7 and day 11 after treatment, five mice in each group were sacrificed, and the wound area was cut for further RT-qPCR, H&E staining, and immunohistochemical staining of CD31.

2.13. Bioluminescence imaging

The survival time of transplanted mAM-MSC (Luc$^+$) in mouse burn wounds was assessed using bioluminescence imaging. Luc$^+$ MSC resuspended in PBS was used as the control. After anesthesia, mice were injected intraperitoneally with 10 μL D-luciferin (150 mg/mL in PBS, Yeasen Biotechnology, China) per gram of mouse weight. Images were obtained with a 3-min exposure to a small animal *in vivo* imaging system (IVScope 8500, Clinx Science Instruments Co., Ltd, China). Images were acquired on days 0, 3, 7, and 9. Bioluminescent photons were measured in each wound area using the Clinx IVScopeEQ Capture software.

2.14. Histological analysis

Hematoxylin and eosin (H&E) staining and CD31 immunohistochemical staining were performed to observe re-epithelialization and vascularization of the burn wound. The wounds together with 2 mm of the surrounding healthy skin edge, were excised and fixed with 10% PFA overnight at 4 °C. After embedding in paraffin, the tissues were cut into sections and stained with an H&E staining kit (Beyotime, China) and a primary antibody against CD31 (1:50, Abcam, USA) to visualize angiogenesis. Re-epithelialization was measured at day 11 by H&E staining. Digital images were obtained and analyzed using Image-Pro Plus Software. Wound edge was calculated by tracing the distance between the leading edges of epithelium within the wound.

2.15. Statistical analysis

All data were statistically analyzed with SPSS 20.0 and presented as mean ± standard deviation (SD). GraphPad Prism 8 software was used for statistical analyses and generation of figures. Differences between two groups were analyzed by two-tailed Student's *t*-test. For multiple comparisons, one-way analysis of variance (ANOVA) and Tukeys multiple comparisons test were used. $P < 0.05$ was considered as statistically significant.

3. Results

3.1. Fabrication of mAM

The mAM was fabricated using our previously described protocol [42]. The general view of the cleaned amniotic membrane was presented in Fig. 1A. The fluorescent images of DAPI indicated that the residual DNA content of the amniotic membrane was eliminated completely after three repetitive freeze-thaw cycles and DNA enzymatic digestion (Fig. 1B). After being decellularized and cut into microparticles, the mAM appeared as white translucent quadrilaterals, with the size of about 400 μm, as measured by bright field image (Fig. 1C).

3.2. Characteristics of mAM-MSC

The SEM images of mAM and mAM-MSC showed obvious differences in surface topography (Fig. 2A). Before co-culturing with MSC, the surface of the mAM was smooth and flat. When co-cultured with MSC for 3 days, the surface of the mAM was attached to the MSC, which maintained a spindle-like stretched shape. Cytoskeleton staining was conducted when mAM-MSC was cultured for 3 or 7 days. Fig. 2B shows that the cytoskeleton was dyed red and had a long spindle shape, extending through the whole cell; however, there were no obvious morphological differences between days 3 and 7. In the CCK8 assay, compared with the control group (traditionally 2D-cultured MSC), OD values in the mAM-MSC group were higher from day 1 to day 7, with an ascending trend (all $P < 0.05$, Fig. 2C). As shown in Fig. 2D, the live/dead staining results showed that MSC adhered to the surface of mAM in the 3D culture system on days 1, 3, and 7, and more cells were detected on mAM after prolonged culture times, especially on days 3 and 7. More importantly, nearly no dead cells, which stained red, were found on mAM during the 7-day culture period.

3.3. Transcriptomic analysis of the effects of mAM on MSC

To further understand the biological effects of mAM on MSC, we conducted RNA-seq transcriptomic analysis to compare the gene expression profile of MSC cultured on mAM (mAM-MSC group) with that of traditional 2D-cultured MSC (MSC group). The results of sample-to-sample cluster analysis are shown in Fig. 3A. A darker blue color indicates smaller distances and fewer differences between the two sequencing samples. Overall, 1785 DEGs were detected in the mAM-MSC group compared with the MSC group, with 773 upregulated and 1012 downregulated genes (Fig. 3B). The heat map in Fig. 3C shows the cluster analysis results of the expression levels of DEGs between the two groups. GO enrichment analysis revealed that DEGs related to cell adhesion (GO:0007155), positive regulation of cell population proliferation (GO:0008284), extracellular matrix (GO:0031 012), cytokine activity (GO:0005125), cytokine-mediated signaling pathway (GO:0019 221), and positive regulation of angiogenesis (GO:0045 788) were all
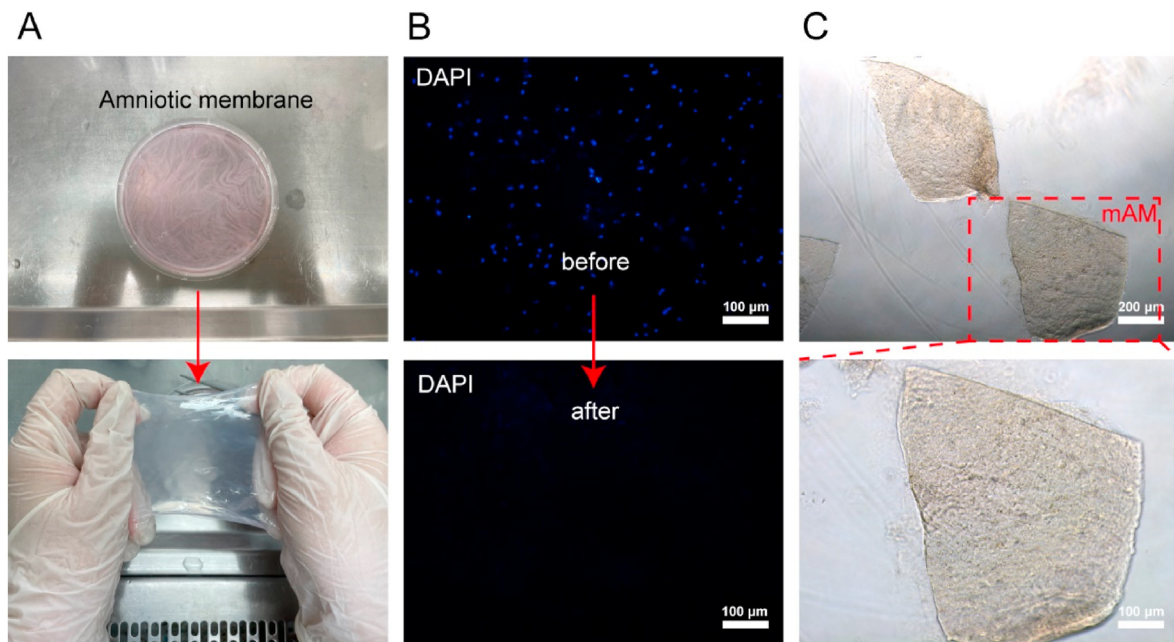
Fig. 1. Fabrication of mAM. (A) General view of the cleaned amniotic membrane. (B) DAPI images of amniotic membrane before and after decellularization. (C) Bright field images of mAM at different magnifications.
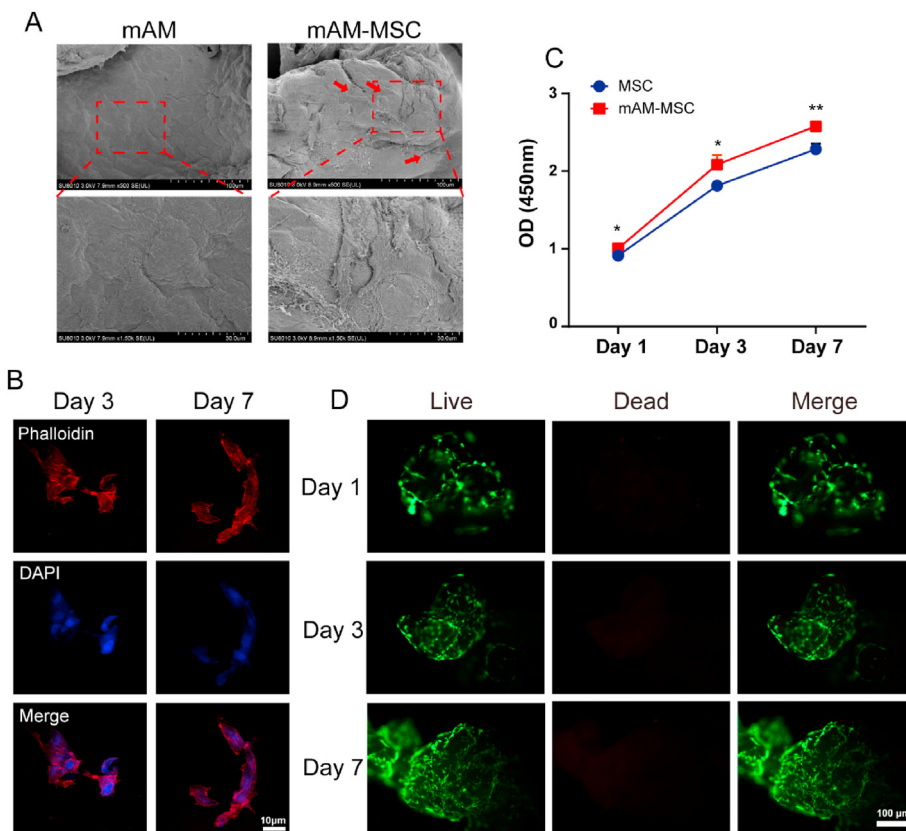

Fig. 2. Characteristics of mAM-MSC. (A) SEM images showing the morphology of mAM and mAM-MSC at different magnifications. Red arrows indicate microscopic MSC. (B) Immunofluorescence images of phalloidin indicating the cytoskeleton of MSC on mAM cultured for 3 and 7 days. (C) Comparing cell proliferation rate of MSC in traditional 2D plate and on mAM by CCK8 assay. (D) Live/dead staining of MSC seeded on mAM on day 1, 3 and 7 using fluorescence microscopy. *$P < 0.05$ and **$P < 0.01$. (For interpretation of the references to colour in this figure legend, the reader is referred to the Web version of this article.)

significantly enriched in the mAM-MSC group compared to those in the MSC group (Fig. 3D). Furthermore, KEGG enrichment analysis indicated that the significantly enriched pathways in the mAM-MSC group compared with the MSC group mainly included cytokine-cytokine receptor interaction (hsa04060), ECM-receptor interaction (hsa04512), the PI3K-Akt signaling pathway (hsa04151), and the VEGF signaling pathway (hsa04370) (Fig. 3E). As shown in Fig. 3F, results of GSEA indicated that some enriched GO terms, especially cell-matrix adhesion (GO:0007160), fibroblast growth factor receptor signaling pathway (GO:0008543), positive regulation of transforming growth factor beta receptor signaling pathway (GO:0030 511), positive regulation of endothelial cell migration (GO:0010 595), blood vessel morphogenesis
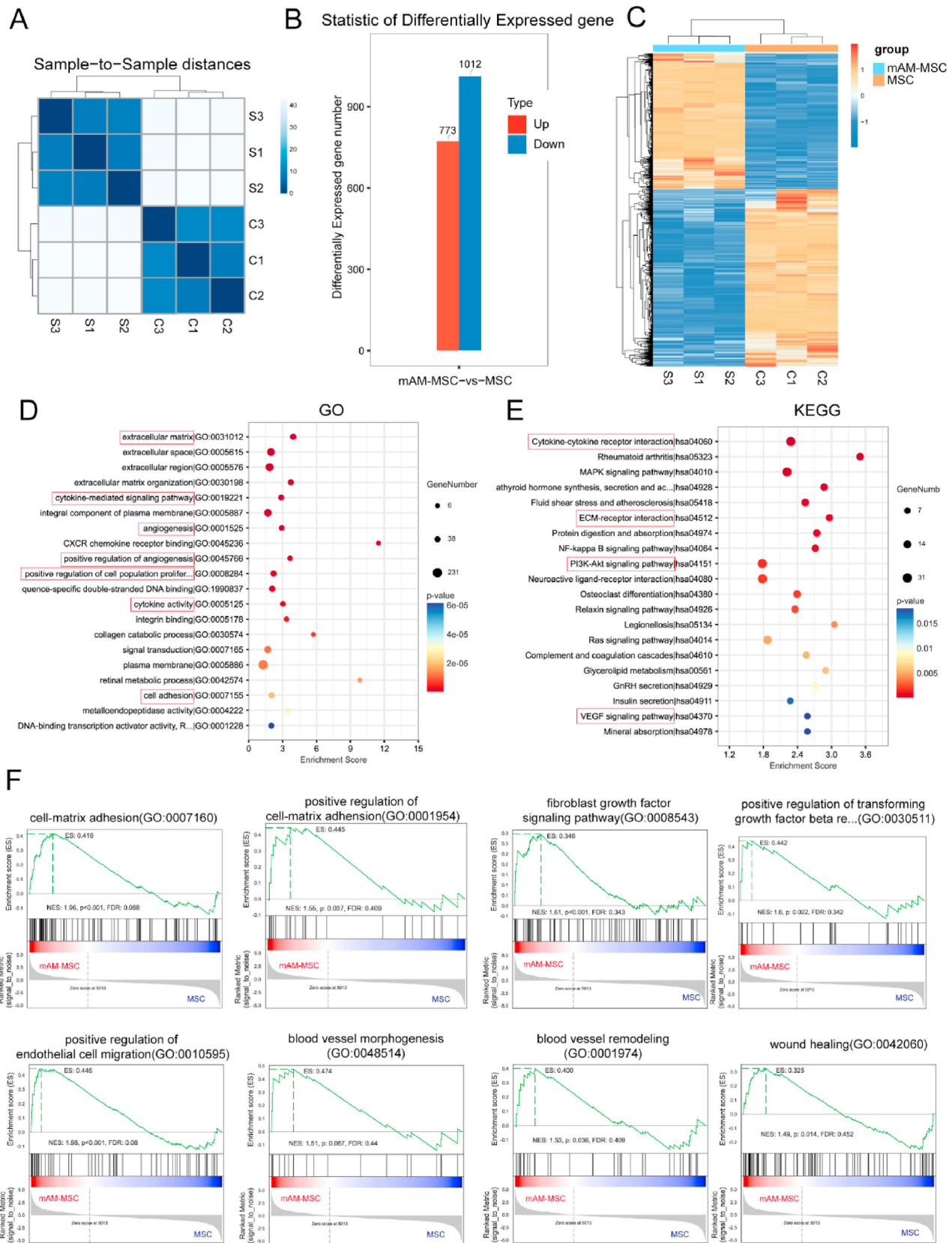
Fig. 3. Bioinformatic analysis of RNA-seq. (A) Sample-to-Sample cluster analysis of sequencing samples in mAM-MSC group and MSC group; C1–C3 refer to three samples in MSC group, and S1–S3 refer to three samples in mAM-MSC group. (B) Statistical graph of DEGs in the two groups. (C) Heat map of gene expression levels of DEGs in the two groups. (D and E) The GO and KEGG enrichment analysis of DEGs of mAM-MSC group vs. MSC group. (F) GSEA based on RNA-Seq data. *P* value < 0.05 and fold change >1.5 or fold change <0.5 was set as the criteria.

(GO:0048 514), blood vessel remodeling (GO:0001974), and wound healing (GO:0042 060), were significantly activated in the mAM-MSC group compared to the MSC group.

From the results of GSEA, considering that three neovascularization-related GO terms (positive regulation of endothelial cell migration, blood vessel morphogenesis, and blood vessel remodeling) were significantly activated in the mAM-MSC group, we further present the expression levels of some DEGs from these GO terms by heatmaps in Fig. 4A. The large number of significantly upregulated genes within these GO terms in the mAM-MSC group contributed to the significant activation of angiogenic functions. In addition, some growth factors that promote angiogenesis and wound healing were highly expressed in the mAM-MSC group, such as VEGF, TGFB1, HGF, FGF, and PDGF (Fig. 4B). In addition, VEGF, TGFB1, IGF1, and ANGPT1 levels were also significantly higher in the mAM-MSC group, as determined by RT-qPCR (all $P < 0.05$, Fig. 4C), validating some of the results in Fig. 4A and B.

3.4. Biological effects of mAM-MSC on HUVECs in vitro

The biological effects of mAM-MSC on the migration and angiogenesis abilities of HUVECs were evaluated using transwell cell migration and tube formation assays. As shown in Fig. 5A, the MSC supernatant
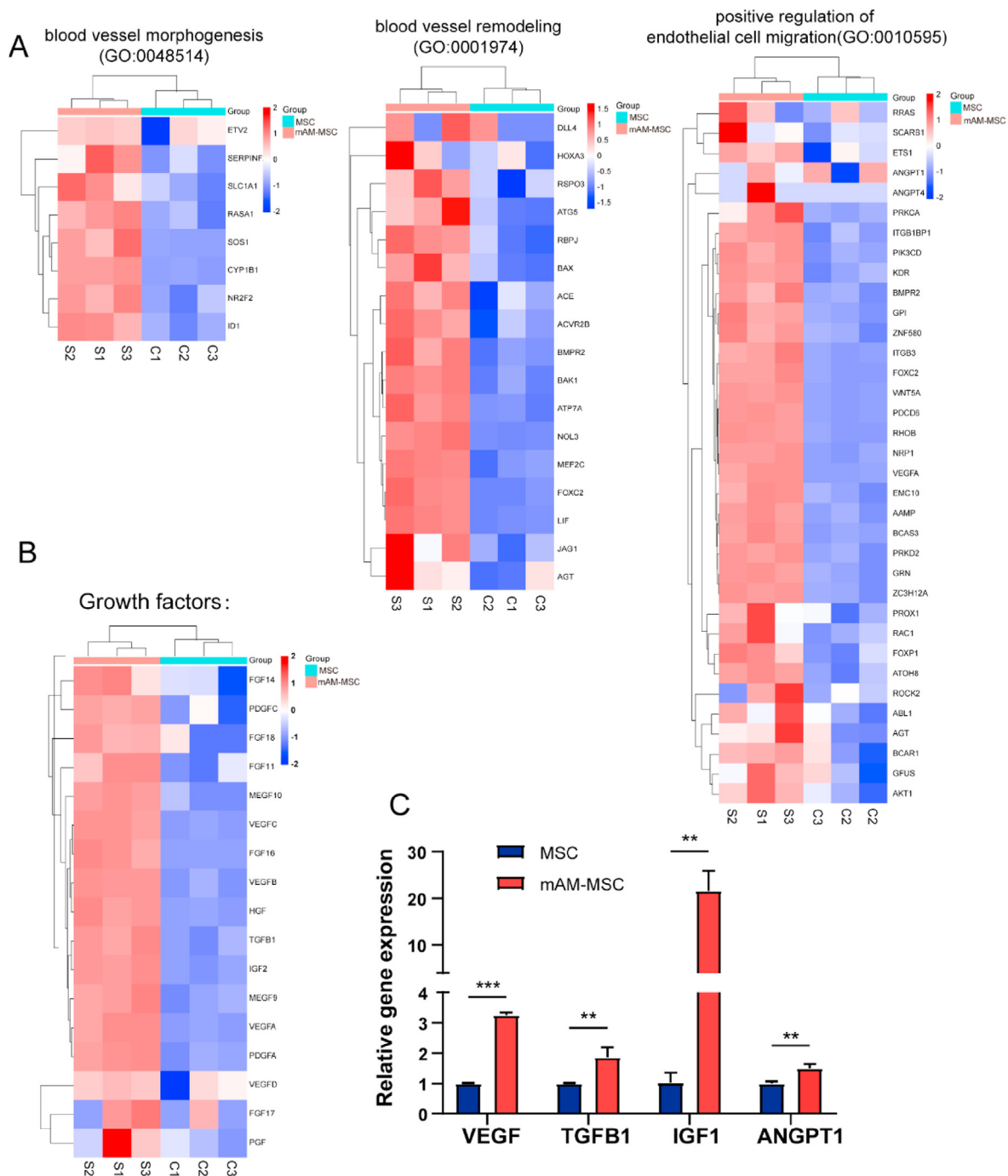

Fig. 4. Angiogenesis-related genes were significantly enriched in mAM-MSC group. (A) Heatmap of genes within some GO terms with angiogenesis functions according to GSEA results. (B) Heatmap of gene expression level of some growth factors based on RNA-seq analysis. (C) RT-qPCR identified the mRNA level of some factors. Error bars represent mean ± SD; n = 3 independent experiments. Significance was determined using *t*-test, *$P < 0.05$, **$P < 0.01$ and ***$P < 0.001$.
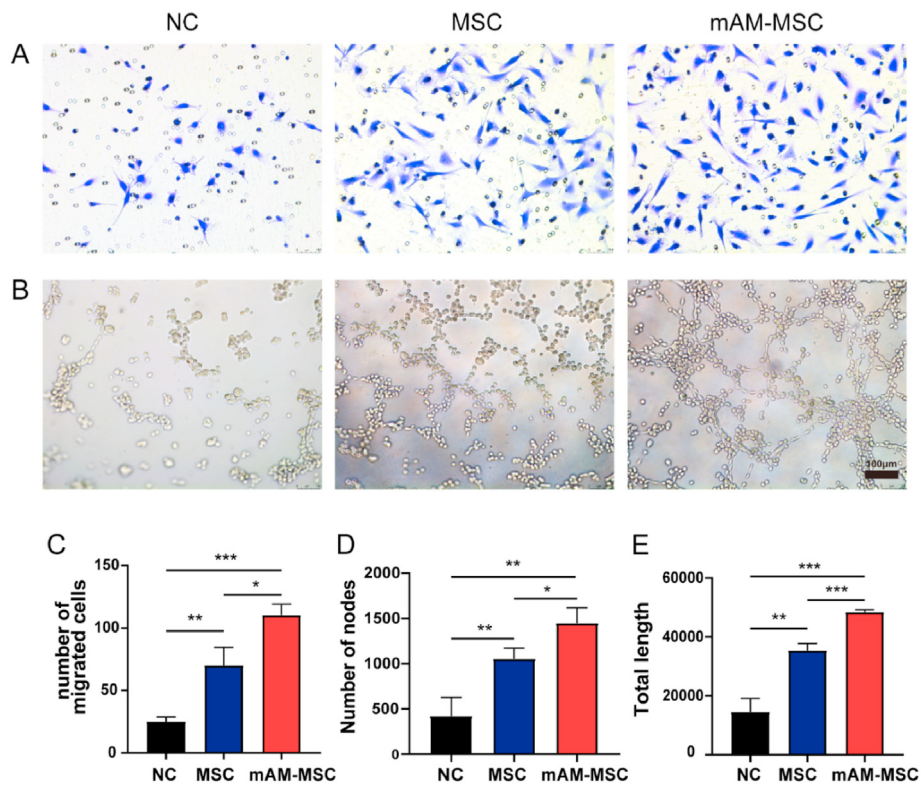
Fig. 5. Biological effects of mAM-MSC on HUVECs *in vitro*. (A) Representative images of transwell assay. (B) Representative images of tube formation assay. (C) Quantification of HUVECs migrated in each group. (D–E) Quantitative analysis of nodes and total length formed in the three groups. NC: high-glucose DMEM. *$P <$ 0.05, **$P <$ 0.01 and ***$P <$ 0.001.
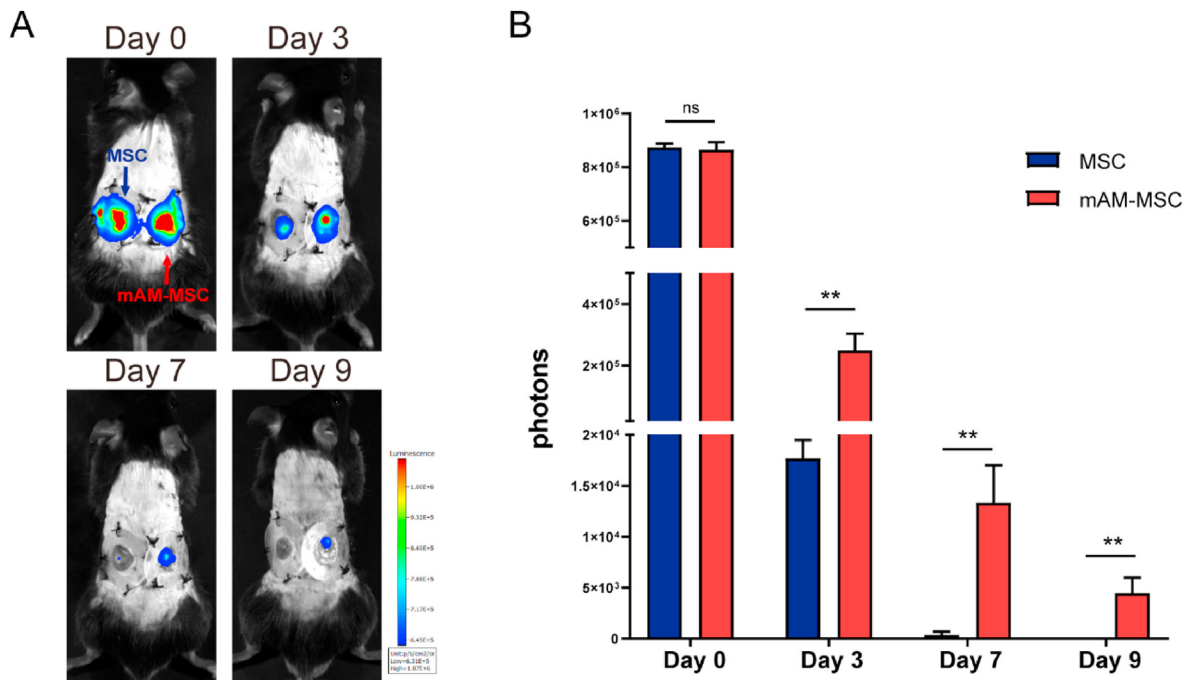

Fig. 6. mAM assisted survival of MSC on burn wound. (A) Representative bioluminescence images in two groups on day 0, 3, 7 and 9. MSC alone was injected into the left wound, and mAM-MSC was applied on the right. (B) Quantitative analysis of the photons on wounds in two groups on day 0, 3, 7 and 9. *$P <$ 0.05 and **$P <$ 0.01.

greatly promoted the migration of HUVECs compared to the NC group ($P <$ 0.01), whereas the supernatant of mAM-MSC drove significantly more cell migration than the MSC group ($P <$ 0.05, Fig. 5C). Moreover, the supernatant of mAM-MSC induced more tubes to form *in vitro* than the

MSC and NC groups (Fig. 5B), showing better capillary-like structures regardless of the number of nodes or the total length (all $P <$ 0.05, Fig. 5D and E).

3.5. mAM assisted survival of MSC on burn wound

To evaluate how long mAM-MSC can survive in burn wound environments, the survival of mAM-MSC in burn wounds was determined using bioluminescence imaging; MSC alone was used as the control. The same amount of Luc$^+$ MSC in the two groups was applied to the bilateral burn wounds of the same mouse on day 0, and the signal intensity was expressed as photons (p/s/cm^2/sr), representing the survival of Luc$^+$ MSC (Fig. 6A). According to the recorded photons, the number of photons in both MSC and mAM-MSC groups decreased at later time points. The number of photons in the MSC group was significantly decreased on day 3 compared to that in the mAM-MSC group ($P < 0.01$) and could not be detected on day 7, whereas Luc$^+$ MSC in the mAM-MSC group remained alive from day 3 to day 7, and slight luminescence could be detected on day 9 compared to that in the MSC group ($P < 0.01$, Fig. 6B).

3.6. mAM-MSC accelerated burn wound healing

The burn wound model was constructed on the dorsal skin of mice (Fig. 7A), and all mice were randomly and equally divided into four groups, including sham, mAM, MSC, and mAM-MSC groups, according to different treatments. As shown in Fig. 7B and C, although there was no significant difference in the remaining wound area among the four groups on day 3, mAM and mAM-MSC adhered to and integrated into the wounds of both groups. On day 7, the remaining wound area of mAM group ($51.06 \pm 4.37\%$, $P < 0.001$) and MSC group ($48.43 \pm 4.81\%$, $P <$

0.0001) was minor when compared to the sham group ($68.57 \pm 6.45\%$), but there was no difference between the two groups ($P > 0.05$). In contrast, the mAM-MSC group presented an enhanced wound closure rate, as 70.63% of the wound area was healed, showing a faster healing rate than the mAM or MSC groups ($P < 0.0001$). On day 11, the mAM-MSC group continued to show significantly faster recovery ($5.03 \pm 2.54\%$) than both the mAM and MSC groups (both $P < 0.0001$), in which $21.54 \pm 4.14\%$ and $19.90 \pm 4.08\%$ wound area remained, respectively. Without treatment, the wound remained at about 35% of unrepaired wound area.

H&E staining of the four groups on day 11 revealed the burn wound healing effects in each group (Fig. 8A). Indicated by black arrows, the average length of the wound edge of the mAM-MSC group (0.53 ± 0.35 mm) was notably lower than that of the mAM group (2.43 ± 0.49 mm, $P < 0.0001$) and MSC group (2.55 ± 0.46 mm, $P < 0.0001$), with both of these groups exhibiting average lengths notably lower than that of sham group (4.13 ± 0.35 mm, $P < 0.0001$; Fig. 8B).

3.7. mAM-MSC promoted vascularization in vivo

In vivo angiogenesis in the wound tissues on day 11 in the four groups was reflected by immunohistochemical staining of CD31. Results showed more vessels in the mAM-MSC group than in the mAM or MSC-only and control groups (Fig. 9A and B). The results of the transcriptional analysis of angiogenesis-related factors by RT-qPCR confirmed that VEGF, TGFB1, ANGPT1, HGF, IGF1, and MMP8 levels were generally higher in the
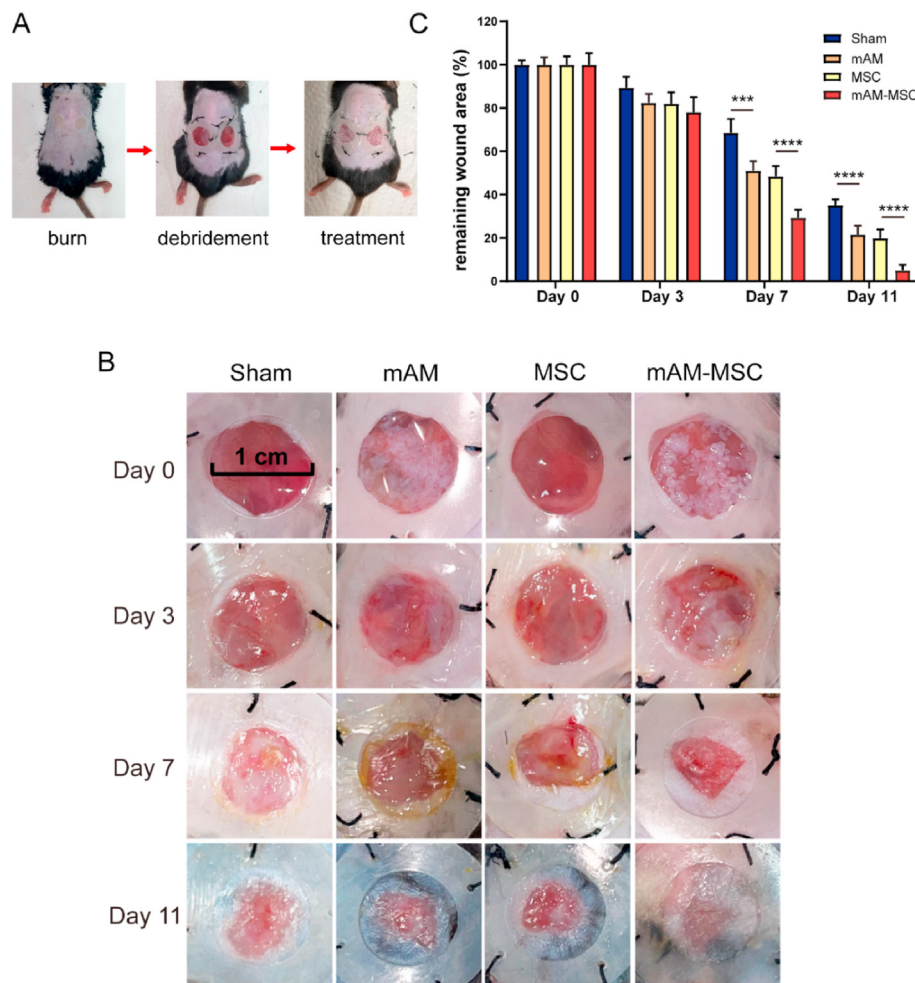

Fig. 7. mAM-MSC accelerated burn wound healing. (A) Schematic diagrams of the burn wound model and treatment. (B) Gross photos of the wound area in four groups on day 0, 3, 7 and 11; (C) Statistical column chart of the remaining wound area in each group. The data are presented as mean ± SD. n = 5. ***$P < 0.001$ and ****$P < 0.0001$.
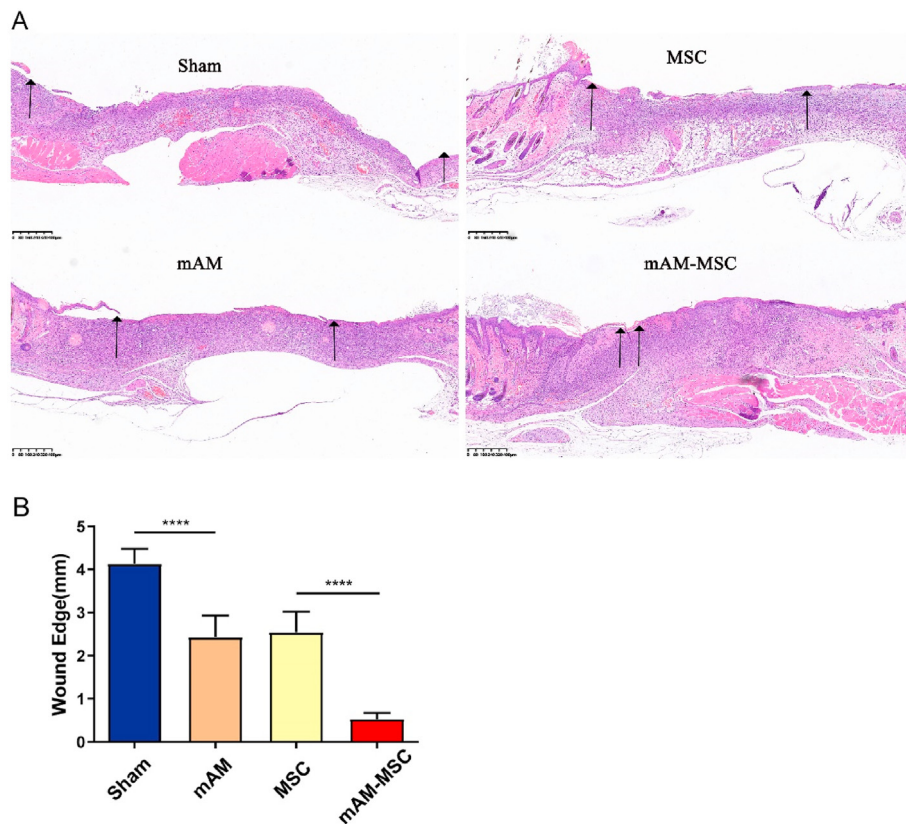
Fig. 8. mAM-MSC accelerated burn wound healing by H&E staining results. (A) Images of H&E staining of the wound tissue sections in four groups on day 11. Black arrows referred to wound edges. Scale bar: 1.25 mm. (B) Quantitative analysis of wound edge on day 11. N = 5. Significance was determined using one-way ANOVA. ****$P < 0.0001$.

mAM-MSC group than in the other three groups (Fig. 9C). This was consistent with the effects of mAM-MSC on promoting angiogenesis and wound healing *in vitro* (Fig. 5B and C).

4. Discussion

Enhanced MSC functionalization in 3D culture environments and how this strategy contributes to safer and better therapeutic outcomes based on MSC has been discussed previously [19]. In this study, we focused on creating a mAM as an ideal 3D cell carrier for UC-MSC to promote rapid cell proliferation and enhance the biological properties of stem cells. mAM-MSC was then applied to burn wounds, achieving long-term survival on the wound surface and accelerating wound healing by promoting neovascularization and re-epithelialization.

Efficient delivery of MSC is an important factor in their medical application. Traditional 2D culture often leads to slow proliferation, low activity, easy differentiation, and loss of cellular stemness in MSC. Eibes et al. found that a microcarrier-based stirred culture system could maximize the *ex vivo* expansion of human MSC, but with additional preparation steps [46]. Carter et al. characterized the impact of the 3D culture environment on the treatment effects of the human MSC secretome on corneal wound healing and found that MSC in 3D conditions performed better, but proliferation in 3D conditions was lower than that in 2D culture [47]. However, in this study, mAM efficiently expanded MSC while enhancing their therapeutic function in 3D culture systems compared to 2D-cultured MSC, as verified by CCK8 and Live/dead staining. The RNA-seq results also confirmed that genes associated with cell adhesion and proliferation were significantly upregulated in the mAM-MSC group. To make mAM a better microcarrier for MSC, emphasis should be put on understanding the supportive effects of mAM on MSC. We suggest the following as likely underlying mechanisms that account

for this. First, as a microcarrier, mAM has a large specific surface area, which provides more space for cell adhesion and growth. Second, the natural cell niche provided by mAM can simulate the *in vivo* cell growth microenvironment, mechanically and biochemically, supporting the adhesion, growth, and proliferation of MSC. Third, automatic expansion of MSC was realized in this study, where the proliferation and passaging of MSC could be easily accomplished by adding new mAM to the 3D culture system without damaging the cells caused by digestive enzymes used in the conventional cell passage method.

Cell survival in the wounded region is another important factor affecting the therapeutic function of MSC. Traditionally, stem cells resuspended in PBS have been directly injected subcutaneously or topically into or around the wound area [48,49]. However, shear stress during the injection process leads to poor cell viability, coupled with a pathogenic wound environment, which is not conducive to cell growth and may lead to apoptosis of a large number of cells and hydrolysis of growth factors in a short time [22]. The low survival rate and tumorigenesis associated with stem cell transplantation have limited the application of stem cells. In our study, the results of bioluminescence imaging demonstrated that mAM-MSC survived longer on the wound than MSC alone. Reasons are as follows. First, mAM not only has the general characteristics of microcarriers, such as a large specific surface area, but also provides a natural environment for MSC to adhere, proliferate, and protect the stem cells from tolerating ischemic and hypoxic conditions in the burn wound after transplantation. Second, the mechanical properties of mAM-MSC allow the cells to be glued onto wounds directly without injection, reducing the harm caused by shear stress from injection.

Improving the paracrine function of MSC is a key factor for their therapeutic functionality. MSC exert therapeutic effects mainly through paracrine secretion, and the role of MSC exosomes in promoting wound
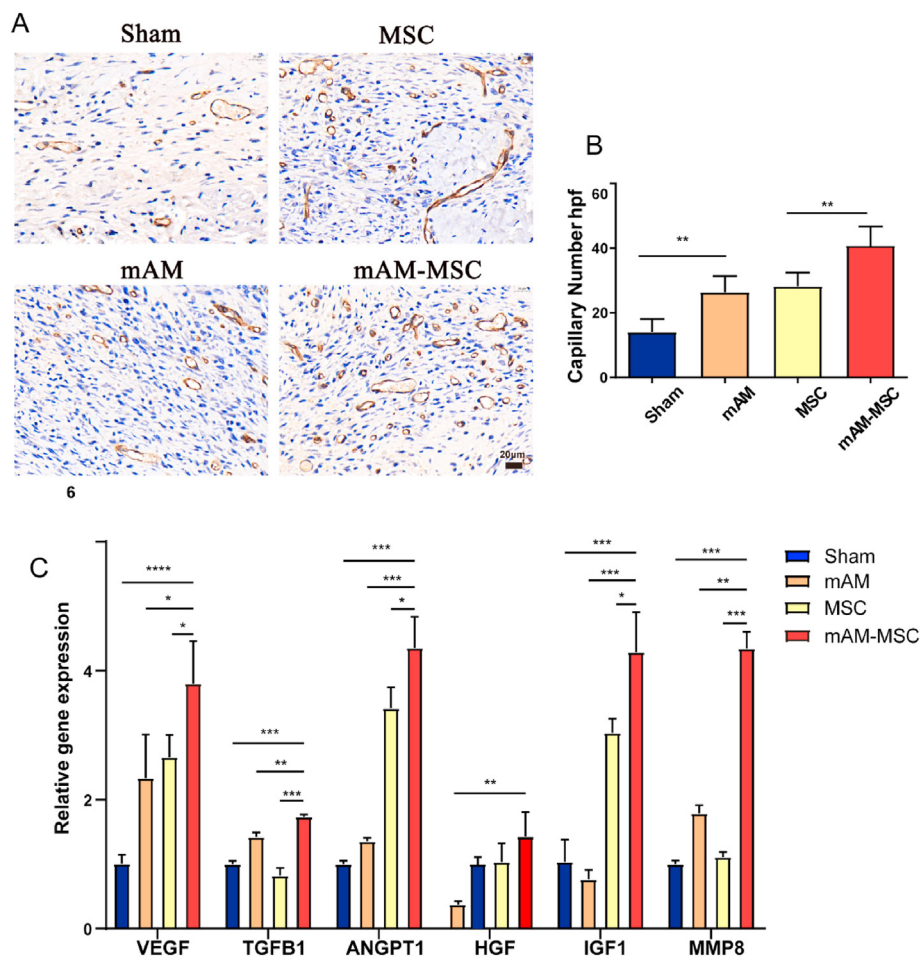
Fig. 9. CD31 staining results and mRNA level of factors *in vivo*. (A–B) Images of immunohistochemical staining of CD31 of the wound tissue sections in four groups on day 11 and quantitative analysis of the capillary hpf. Error bars represent mean $\pm$ SD; n = 5. Significance was determined using one-way ANOVA. (C) RT-qPCR identifies the mRNA level of some factors of the wounds on day 7. Significance was determined using one-way ANOVA. *$P < 0.05$, **$P < 0.01$, ***$P < 0.001$ and ****$P < 0.0001$.

healing has been widely recognized [9–11,50–54]. Studies have shown that the paracrine function of stem cells is influenced by the culture environment [55,56]. In this study, we demonstrated that mAM can improve the biological functions of MSC by manipulating the secretion profiles of many wound healing-related factors and cytokines. As shown in the RNA-seq results, genes involved in growth factors, cytokine activity, angiogenesis, ECM organization, and wound healing were significantly upregulated in the mAM-MSC group, especially genes encoding growth factors, such as VEGF, TGFB1, FGF, HGF, PDGF, and IGF1, the upregulation of which was verified via RT-qPCR (Fig. 4C). Therefore, RNA-seq and RT-qPCR results could explain the enhanced angiogenic effects observed in the migration and tube formation assays of HUVEC *in vitro* (Fig. 5), as well as the angiogenesis and wound healing effects in the burn wound model *in vivo* (Figs. 7–9). We have several hypotheses to explain these findings. First, mAM, a natural membrane rich in ECM, might play a significant role in ECM-cell interactions to stimulate the elevated expression of growth factors in MSC. Second, human amniotic membrane contains many growth factors, such as EGF, KGF, HGF, bFGF, VEGF, PDGF, TGF-beta1, -beta2, and -beta3 [31], which may give positive feedback to cells on secretion. Third, the 3D culture microenvironment provides a more dynamic space for the cells to stretch. Direct cell-cell communication between MSC may improve their paracrine effects. In addition, the 3D culture system promoted better nutrient intake and gas exchange by the MSC, thereby improving cell secretion.

After proving the improved biological properties of mAM-MSC *in vitro*, to comprehensively study the therapeutic function of mAM-MSC, we employed mAM-MSC on a mouse burn wound model. The results of H&E and CD31 staining showed that the mAM-MSC group had positive therapeutic effects on wound healing, with faster re-epithelialization and

better angiogenesis in the wound (Figs. 8–9). These effects can be explained as follows. First, the survival time of MSC in this group was the longest (9 days), which means its pro-healing effect can last longer. Second, the natural ECM composition and basement structure of the amniotic membrane can mimic a dermal scaffold, inducing skin cell self-repair and regeneration. Third, high expression of growth factors, such as VEGF and HGF, promotes wound healing and blood vessel morphogenesis. We then investigated the expression of certain factors in the wound tissue and found that VEGF, TGFB1, ANGPT1, HGF, IGF1, and MMP8 expression was significantly upregulated in the mAM-MSC group on day 7 (Fig. 9C). Wound healing and angiogenesis involve a substantial number of signaling proteins, such as chemokines, cytokines, growth factors (GFs), and matrix metalloproteinases (MMPs) [52,57–59]. VEGF, TGFB1, and HGF are widely recognized for their ability to repair and regenerate the dermis and epidermis, regulate inflammation, and promote angiogenesis. Irina et al. assessed the effect of VEGF secreted by MSC spheroids in promoting angiogenesis and maintaining MSC viability and migration [54], the results of which were consistent with those of our study. ANGPT1 plays an important role in angiogenesis, assisting in survival, inhibiting the apoptosis of vascular endothelial cells, and preserving vascular stability [60]. IGF1 can also facilitate cell proliferation and angiogenesis. MMPs play a key role in the remodeling of connective tissue, and MMP8 has been shown to be beneficial for angiogenesis [61, 62]. Wei et al. found that MSC enhanced diabetic foot ulcer (DFU) wound healing by increasing MMP-8 expression [61]. Fang et al. verified that MMP8 knockdown in HUVEC decreased the proliferation and migration ability of cells, decreased the formation of capillary-like networks *in vitro*, and impaired their capacity for *in vivo* angiogenesis [62].

5. Conclusion

In this study, we constructed mAM-MSC and evaluated their pro-healing and angiogenic effects in a burn-wound model. After a series of experimental validations, we found that mAM could achieve efficient MSC expansion *in vitro* and maintain high cellular activity both *in vitro* and in burn wounds. The expression levels of growth factors and other proteins related to wound healing and angiogenesis were significantly increased in the mAM-MSC. The application of mAM-MSC to burn wounds significantly increased the healing rate and number of blood vessels in burn wounds.

Credit author statement

ZYJ and XSC contributed to the conception and design. ZZX, XJN and WCH contributed to the data, analysis and interpretation. ZZX and ZYJ contributed to the manuscript writing. ZZX, XJN, WCH and JC contributed to the animal experiments. ZYJ, XSC and JSZ contributed to the manuscript revision. SFT, WYX and CH provided the study materials. ZYJ and XSC contributed to the conception and design, financial support, and final approval of the manuscript. The authors read and approved the final manuscript.

Declaration of competing interest

The authors declare that they have no known competing financial interests or personal relationships that could have appeared to influence the work reported in this paper.

Data availability

Data will be made available on request.

Acknowledgements

References

[1] Y. Yao, A. Zhang, C. Yuan, X. Chen, Y. Liu, Recent trends on burn wound care: hydrogel dressings and scaffolds, Biomater. Sci. 9 (13) (2021) 4523–4540.

[2] M. Burgess, F. Valdera, D. Varon, E. Kankuri, K. Nuutila, The immune and regenerative response to burn injury, Cells 11 (19) (2022).

[3] G.E.B. M, L. Dosh, H. Haidar, A. Gerges, S. Baassiri, A. Leone, F. Rappa, A. Jurjus, Nerve Growth Factor and Burn Wound Healing: Update of Molecular Interactions with Skin Cells, Burns, 2022.

[4] G.C. Gurtner, S. Werner, Y. Barrandon, M.T. Longaker, Wound repair and regeneration, Nature 453 (7193) (2008) 314–321.

[5] V. Singh, L. Devgan, S. Bhat, S.M. Milner, The pathogenesis of burn wound conversion, Ann. Plast. Surg. 59 (1) (2007) 109–115.

[6] K.A.A. Kwa, H. Goei, R.S. Breederveld, E. Middelkoop, C.H. van der Vlies, M.E. van Baar, A systematic review on surgical and nonsurgical debridement techniques of burn wounds, J. Plast. Reconstr. Aesthetic Surg. 72 (11) (2019) 1752–1762.

[7] W. Liu, M. Yu, D. Xie, L. Wang, C. Ye, Q. Zhu, F. Liu, L. Yang, Melatonin-stimulated MSC-derived exosomes improve diabetic wound healing through regulating macrophage M1 and M2 polarization by targeting the PTEN/AKT pathway, Stem Cell Res. Ther. 11 (1) (2020) 259.

[8] J. Wang, D. Zhang, Y. Zhu, X. Mo, P.C. McHugh, Q. Tong, Astragalus and human mesenchymal stem cells promote wound healing by mediating immunomodulatory effects through paracrine signaling, Regen. Med. 17 (4) (2022) 219–232.

[9] J. Yang, Z. Chen, D. Pan, H. Li, J. Shen, Umbilical cord-derived mesenchymal stem cell-derived exosomes combined pluronic F127 hydrogel promote chronic diabetic wound healing and complete skin regeneration, Int. J. Nanomed. 15 (2020) 5911–5926.

[10] R. Guillamat-Prats, The role of MSC in wound healing, scarring and regeneration, Cells 10 (7) (2021).

[11] B. Zhang, X. Wu, X. Zhang, Y. Sun, Y. Yan, H. Shi, Y. Zhu, L. Wu, Z. Pan, W. Zhu, H. Qian, W. Xu, Human umbilical cord mesenchymal stem cell exosomes enhance angiogenesis through the Wnt4/β-catenin pathway, Stem Cells Transl Med 4 (5) (2015) 513–522.

[12] W. Zhao, R. Zhang, C. Zang, L. Zhang, R. Zhao, Q. Li, Z. Yang, Z. Feng, W. Zhang, R. Cui, Exosome derived from mesenchymal stem cells alleviates pathological scars by inhibiting the proliferation, migration and protein expression of fibroblasts via delivering miR-138-5p to target SIRT1, Int. J. Nanomed. 17 (2022) 4023–4038.

[13] A. Surowiecka, A. Chrapusta, M. Klimeczek-Chrapusta, T. Korzeniowski, J. Drukała, J. Strużyna, Mesenchymal stem cells in burn wound management, Int. J. Mol. Sci. 23 (23) (2022).

[14] M. Wang, X. Xu, X. Lei, J. Tan, H. Xie, Mesenchymal stem cell-based therapy for burn wound healing, Burns Trauma 9 (2021) tkab002.

[15] C.T. Huerta, F.A. Voza, Y.Y. Ortiz, Z.J. Liu, O.C. Velazquez, Mesenchymal stem cell-based therapy for non-healing wounds due to chronic limb-threatening ischemia: a review of preclinical and clinical studies, Front Cardiovasc Med 10 (2023), 1113982.

[16] M.J. Saadh, A.A. Ramírez-Coronel, R.S. Saini, J.L. Arias-Gonzáles, A.H. Amin, J.C.O. Gavilán, I. Sàrbu, Advances in mesenchymal stem/stromal cell-based therapy and their extracellular vesicles for skin wound healing, Hum. Cell (2023).doi: 10.1007/s13577-023-00904-8. Online ahead of print.

[17] L. Zhou, H. Wang, S. Yao, L. Li, X. Kuang, Efficacy of human adipose derived mesenchymal stem cells in promoting skin wound healing, J Healthc Eng 2022 (2022), 6590025.

[18] A. Kerstan, K. Dieter, E. Niebergall-Roth, S. Klingele, M. Jünger, C. Hasslacher, G. Daeschlein, L. Stemler, U. Meyer-Pannwitt, K. Schubert, G. Klausmann, T. Raab, M. Goebeler, K. Kraft, J. Esterlechner, H.M. Schröder, S. Sadeghi, S. Ballikaya, M. Gasser, A.M. Waaga-Gasser, G.F. Murphy, D.P. Orgill, N.Y. Frank, C. Ganss, K. Scharffetter-Kochanek, M.H. Frank, M.A. Kluth, Translational development of ABCB5(+) dermal mesenchymal stem cells for therapeutic induction of angiogenesis in non-healing diabetic foot ulcers, Stem Cell Res. Ther. 13 (1) (2022) 455.

[19] D. Kouroupis, D. Correa, Increased mesenchymal stem cell functionalization in three-dimensional manufacturing settings for enhanced therapeutic applications, Front. Bioeng. Biotechnol. 9 (2021), 621748.

[20] Y. Shou, L. Liu, Q. Liu, Z. Le, K.L. Lee, H. Li, X. Li, D.Z. Koh, Y. Wang, T.M. Liu, Z. Yang, C.T. Lim, C. Cheung, A. Tay, Mechano-responsive hydrogel for direct stem cell manufacturing to therapy, Bioact. Mater. 24 (2023) 387–400.

[21] P. Rybkowska, K. Radoszkiewicz, M. Kawalec, D. Dymkowska, B. Zabłocka, K. Zabłocki, A. Sarnowska, The metabolic changes between monolayer (2D) and three-dimensional (3D) culture conditions in human mesenchymal stem/stromal cells derived from adipose tissue, Cells 12 (1) (2023).

[22] B.A. Aguado, W. Mulyasasmita, J. Su, K.J. Lampe, S.C. Heilshorn, Improving viability of stem cells during syringe needle flow through the design of hydrogel cell carriers, Tissue Eng. 18 (7–8) (2012) 806–815.

[23] M. Mytsyk, G. Cerino, G. Reid, L.G. Sole, F.S. Eckstein, D. Santer, A. Marsano, Long-term severe in vitro hypoxia exposure enhances the vascularization potential of human adipose tissue-derived stromal vascular fraction cell engineered tissues, Int. J. Mol. Sci. 22 (15) (2021).

[24] B. Koh, N. Sulaiman, M.B. Fauzi, J.X. Law, M.H. Ng, R.B.H. Idrus, M.D. Yazid, Three dimensional microcarrier system in mesenchymal stem cell culture: a systematic review, Cell Biosci. 10 (2020) 75.

[25] A. YekrangSafakar, A. Acun, J.W. Choi, E. Song, P. Zorlutuna, K. Park, Hollow microcarriers for large-scale expansion of anchorage-dependent cells in a stirred bioreactor, Biotechnol. Bioeng. 115 (7) (2018) 1717–1728.

[26] M. Chen, X. Wang, Z. Ye, Y. Zhang, Y. Zhou, W.S. Tan, A modular approach to the engineering of a centimeter-sized bone tissue construct with human amniotic mesenchymal stem cells-laden microcarriers, Biomaterials 32 (30) (2011) 7532–7542.

[27] P. Fuentes, M.J. Torres, R. Arancibia, F. Aulestia, M. Vergara, F. Carrión, N. Osses, C. Altamirano, Dynamic culture of mesenchymal stromal/stem cell spheroids and secretion of paracrine factors, Front. Bioeng. Biotechnol. 10 (2022), 916229.

[28] J.Y. Kim, W.K. Rhim, S.G. Cha, J. Woo, J.Y. Lee, C.G. Park, D.K. Han, Bolstering the secretion and bioactivities of umbilical cord MSC-derived extracellular vesicles with 3D culture and priming in chemically defined media, Nano Converg 9 (1) (2022) 57.

[29] Y. Zeng, L. Zhu, Q. Han, W. Liu, X. Mao, Y. Li, N. Yu, S. Feng, Q. Fu, X. Wang, Y. Du, R.C. Zhao, Preformed gelatin microcryogels as injectable cell carriers for enhanced skin wound healing, Acta Biomater. 25 (2015) 291–303.

[30] I. Mawji, E.L. Roberts, T. Dang, B. Abraham, M.S. Kallos, Challenges and opportunities in downstream separation processes for mesenchymal stromal cells cultured in microcarrier-based stirred suspension bioreactors, Biotechnol. Bioeng. 119 (11) (2022) 3062–3078.

[31] J.P. Bennett, R. Matthews, W.P. Faulk, Treatment of chronic ulceration of the legs with human amnion, Lancet 1 (8179) (1980) 1153–1156.

[32] W.P. Faulk, R. Matthews, P.J. Stevens, J.P. Bennett, H. Burgos, B.L. Hsi, Human amnion as an adjunct in wound healing, Lancet 1 (8179) (1980) 1156–1158.

[33] M. Garoufalis, D. Nagesh, P.J. Sanchez, R. Lenz, S.J. Park, J.G. Ruff, A. Tien, J. Goldsmith, A. Seat, Use of dehydrated human amnion/chorion membrane allografts in more than 100 patients with six major types of refractory nonhealing wounds, J. Am. Podiatr. Med. Assoc. 108 (2) (2018) 84–89.

[34] J. Chen, C.D. Lopez, A.O. Girard, M. Abousy, R.J. Redett, M. Groves, R. Yang, Dehydrated human amnion/chorion membrane allografts for myelomeningocele and wound reconstruction, Childs Nerv Syst 37 (12) (2021) 3721–3731.

[35] K. Jirsova, G.L.A. Jones, Amniotic membrane in ophthalmology: properties, preparation, storage and indications for grafting-a review, Cell Tissue Bank. 18 (2) (2017) 193–204.

[36] M. Nogami, T. Kimura, S. Seki, Y. Matsui, T. Yoshida, C. Koike-Soko, M. Okabe, H. Motomura, R. Gejo, T. Nikaido, A human amnion-derived extracellular matrix-coated cell-free scaffold for cartilage repair: in vitro and in vivo studies, Tissue Eng. 22 (7–8) (2016) 680–688.

[37] A. Ilhan, U. Yolcu, F.C. Gundogan, Amniotic membrane: new concepts for an old dressing, Wound Repair Regen. 23 (1) (2015) 145.

[38] B.J. Cox, A. Ralston, The amnion as a window into human pluripotency, Cell Stem Cell 29 (5) (2022) 661–662.

[39] N.G. Fairbairn, M.A. Randolph, R.W. Redmond, The clinical applications of human amnion in plastic surgery, J. Plast. Reconstr. Aesthetic Surg. 67 (5) (2014) 662–675.

[40] H. Bakhtiar, A. Ashoori, S. Rajabi, M. Pezeshki-Modaress, A. Ayati, M.R. Mousavi, M.R. Ellini, A. Kamali, A. Azarpazhooh, A. Kishen, Human amniotic membrane extracellular matrix scaffold for dental pulp regeneration in vitro and in vivo, Int. Endod. J. 55 (4) (2022) 374–390.

[41] Y. Zheng, S. Ji, H. Wu, S. Tian, Y. Zhang, L. Wang, H. Fang, P. Luo, X. Wang, X. Hu, S. Xiao, Z. Xia, Topical administration of cryopreserved living micronized amnion accelerates wound healing in diabetic mice by modulating local microenvironment, Biomaterials 113 (2017) 56–67.

[42] S.Z. Ji, S.C. Xiao, P.F. Luo, G.F. Huang, G.Y. Wang, S.H. Zhu, M.J. Wu, Z.F. Xia, An epidermal stem cells niche microenvironment created by engineered human amniotic membrane, Biomaterials 32 (31) (2011) 7801–7811.

[43] J. Ma, J. Wu, H. Zhang, L. Du, H. Zhuang, Z. Zhang, B. Ma, J. Chang, C. Wu, 3D printing of diatomite incorporated composite scaffolds for skin repair of deep burn wounds, Int J Bioprint 8 (3) (2022) 580.

[44] M. Zaborowska, F. Vazirisani, F.A. Shah, R. Firdaus, O. Omar, K. Ekström, M. Trobos, P. Thomsen, Immunomodulatory effects exerted by extracellular vesicles from Staphylococcus epidermidis and Staphylococcus aureus isolated from bone-anchored prostheses, Biomaterials 278 (2021), 121158.

[45] K.A. Patel, N. Patel, G.H. Kim, L.S. Chape, K.G.D. Agbon, M.P. Angulo Fuentes, F.L. Barbosa, R.T. Castellano, G.N. Gonzalez, S. Mathew, G. Mantile-Selvaggi, R. Reich-Slotky, Validation of automated fluorescent-based technology for measuring total nucleated cell viability of hematopoietic progenitor cell products, Transfusion 62 (4) (2022) 848–856.

[46] G. Eibes, F. dos Santos, P.Z. Andrade, J.S. Boura, M.M. Abecasis, C.L. da Silva, J.M. Cabral, Maximizing the ex vivo expansion of human mesenchymal stem cells using a microcarrier-based stirred culture system, J. Biotechnol. 146 (4) (2010) 194–197.

[47] K. Carter, H.J. Lee, K.S. Na, G.M. Fernandes-Cunha, I.J. Blanco, A. Djalilian, D. Myung, Characterizing the impact of 2D and 3D culture conditions on the therapeutic effects of human mesenchymal stem cell secretome on corneal wound healing in vitro and ex vivo, Acta Biomater. 99 (2019) 247–257.

[48] D. Duscher, J. Barrera, V.W. Wong, Z.N. Maan, A.J. Whittam, M. Januszyk, G.C. Gurtner, Stem cells in wound healing: the future of regenerative medicine? A Mini-Review, Gerontology. 62 (2) (2016) 216–225.

[49] G.T. Kirby, S.J. Mills, A.J. Cowin, L.E. Smith, Stem cells for cutaneous wound healing, BioMed Res. Int. 2015 (2015), 285869.

[50] J.Y. Li, K.K. Ren, W.J. Zhang, L. Xiao, H.Y. Wu, Q.Y. Liu, T. Ding, X.C. Zhang, W.J. Nie, Y. Ke, K.Y. Deng, Q.W. Liu, H.B. Xin, Human amniotic mesenchymal stem cells and their paracrine factors promote wound healing by inhibiting heat stress-induced skin cell apoptosis and enhancing their proliferation through activating PI3K/AKT signaling pathway, Stem Cell Res. Ther. 10 (1) (2019) 247.

[51] D.H. Ha, H.K. Kim, J. Lee, H.H. Kwon, G.H. Park, S.H. Yang, J.Y. Jung, H. Choi, J.H. Lee, S. Sung, Y.W. Yi, B.S. Cho, Mesenchymal stem/stromal cell-derived exosomes for immunomodulatory therapeutics and skin regeneration, Cells 9 (5) (2020).

[52] J.R. Yi, Z.N. Li, H.Q. Xie, B.M. Chen, L. Jiang, L.X. Qian, H.G. Xu, S.R. Li, Z.Z. Lei, J.D. Chen, J. Zhou, [Effects and mechanism of human umbilical vein endothelial cells-derived exosomes on wound healing in diabetic rabbits], Zhonghua Shaoshang Zazhi 38 (11) (2022) 1023–1033.

[53] M. Yu, W. Liu, J. Li, J. Lu, H. Lu, W. Jia, F. Liu, Exosomes derived from atorvastatin-pretreated MSC accelerate diabetic wound repair by enhancing angiogenesis via AKT/eNOS pathway, Stem Cell Res. Ther. 11 (1) (2020) 350.

[54] I. Kozhukharova, N. Minkevich, L. Alekseenko, A. Domnina, O. Lyublinskaya, Paracrine and autocrine effects of VEGF are enhanced in human eMSC spheroids, Int. J. Mol. Sci. 23 (22) (2022).

[55] N. Su, P.L. Gao, K. Wang, J.Y. Wang, Y. Zhong, Y. Luo, Fibrous scaffolds potentiate the paracrine function of mesenchymal stem cells: a new dimension in cell-material interaction, Biomaterials 141 (2017) 74–85.

[56] T. Hou, M. Du, X. Gao, M. An, Human vascular endothelial cells promote the secretion of vascularization factors and migration of human skin fibroblasts under Co-culture and its preliminary application, Int. J. Mol. Sci. 23 (22) (2022).

[57] Y. Guo, G. Chu, W. Cai, Y. Li, X. Lan, J. Li, L. Du, J. Yang, Beneficial effects of oleosomes fused with human fibroblast growth factor 1 on wound healing via the promotion of angiogenesis, Int. J. Mol. Sci. 23 (21) (2022).

[58] J. Holoubek, B. Lipový, M. Knoz, T. Kempný, R. Chaloupková, J. Damborský, L. Vojtová, The Future for the Application of Fibroblast Growth Factor 2 in Modern Wound Healing, Burns, 2022.

[59] Y. Zhang, Y.Y. Zhang, Z.W. Pan, Q.Q. Li, L.H. Sun, X. Li, M.Y. Gong, X.W. Yang, Y.Y. Wang, H.D. Li, L.N. Xuan, Y.C. Shao, M.M. Li, M.Y. Zhang, Q. Yu, Z. Li, X.F. Zhang, D.H. Liu, Y.M. Zhu, Z.Y. Tan, Y.Y. Zhang, Y.Q. Liu, Y. Zhang, L. Jiao, B.F. Yang, GDF11 promotes wound healing in diabetic mice via stimulating HIF-1α-VEGF/SDF-1α-mediated endothelial progenitor cell mobilization and neovascularization, Acta Pharmacol. Sin. 44 (5) (2022) 999–1013.

[60] P. Saharinen, L. Eklund, K. Alitalo, Therapeutic targeting of the angiopoietin-TIE pathway, Nat. Rev. Drug Discov. 16 (9) (2017) 635–661.

[61] L. Wei, Y. Xu, L. Zhang, L. Yang, R.C. Zhao, D. Zhao, Mesenchymal stem cells promote wound healing and effects on expression of matrix metalloproteinases-8 and 9 in the wound tissue of diabetic rats, Stem Cell. Dev. 32 (1-2) (2022) 25–31.

[62] C. Fang, G. Wen, L. Zhang, L. Lin, A. Moore, S. Wu, S. Ye, Q. Xiao, An important role of matrix metalloproteinase-8 in angiogenesis in vitro and in vivo, Cardiovasc. Res. 99 (1) (2013) 146–155.